

Accepted Manuscript

Adaptive Backstepping Control for Air-Breathing Hypersonic Vehicles with Input Nonlinearities

Qinglei Hu, Yao Meng, Chenliang Wang, Youmin Zhang

PII: S1270-9638(17)31843-6
DOI: <https://doi.org/10.1016/j.ast.2017.12.001>
Reference: AESCTE 4323

To appear in: *Aerospace Science and Technology*

Received date: 10 October 2017
Revised date: 21 November 2017
Accepted date: 1 December 2017

Please cite this article in press as: Q. Hu et al., Adaptive Backstepping Control for Air-Breathing Hypersonic Vehicles with Input Nonlinearities, *Aerosp. Sci. Technol.* (2017), <https://doi.org/10.1016/j.ast.2017.12.001>

This is a PDF file of an unedited manuscript that has been accepted for publication. As a service to our customers we are providing this early version of the manuscript. The manuscript will undergo copyediting, typesetting, and review of the resulting proof before it is published in its final form. Please note that during the production process errors may be discovered which could affect the content, and all legal disclaimers that apply to the journal pertain.



Adaptive Backstepping Control for Air-Breathing Hypersonic Vehicles with Input Nonlinearities

Qinglei Hu, Yao Meng, Chenliang Wang

School of Automation Science and Electrical Engineering, Beihang University, Beijing 100191, China

Youmin Zhang

Department of Mechanical, Industrial and Aerospace Engineering, Concordia University, Montreal, Quebec H3G 1M8, Canada

Abstract: This paper addresses the control problem of air-breathing hypersonic vehicles subject to input nonlinearities, aerodynamic uncertainties and flexible modes. An adaptive backstepping controller and a dynamic inverse controller are developed for the altitude subsystem and the velocity subsystem, respectively, where the former eliminates the problem of “explosion of terms” inherent in backstepping control. Moreover, a modified smooth inverse of the dead-zone is proposed to compensate for the dead-zone effects and reduce the computational burden. Based on this smooth inverse, an input nonlinear pre-compensator is designed to handle input saturation and dead-zone nonlinearities, which leads to a simpler control design for the altitude subsystem subject to these two input nonlinearities. It is proved that the proposed controllers can guarantee that all closed-loop signals are bounded and the tracking errors converge to an arbitrarily small residual set. Simulation results are carried out to demonstrate the effectiveness of the proposed control scheme.

Key words: hypersonic vehicle; flexible modes; input nonlinearities; dead-zone; input saturation.

I. Introduction

Air-breathing hypersonic vehicles (AHVs) have received tremendous attention in recent years, since such vehicles have been viewed as the next critical step toward achieving the reliable and cost-efficient access to space and possessing the ability of prompt global strike. The emergence of AHVs benefits a lot from the state-of-the-art technologies, such as ram/scramjet propulsion, high temperature material, thermal protection system, etc. Despite the progress of these advanced technologies, the design of the control schemes for AHVs is still an open problem, owing to the significant flexible effects aroused by their slender geometry and light structure, and the input nonlinearities such as input saturation and dead-zone.

During the past decades, the problem of longitudinal control design for AHVs has been extensively

investigated. Schmidt [1, 2] proposed a multivariable and classic linear control for the linearized longitudinal model of the vehicles developed by Chavez and Schmidt [3, 4]. Later, some similar works have also been presented in [5-7]. However, to guarantee a desirable control performance, these control schemes developed based on a linearized model are always designed by combining the gain scheduling technique, which inevitably requires massive testing and offline analysis. To remedy this, extensive efforts have been devoted to developing control algorithms directly for nonlinear models of AHVs. For instance, in [8], a state-feedback controller was designed by incorporating feedback linearization and disturbance observer-based control. Wu et al. [9] proposed a robust backstepping control approach for a flexible AHV in the presence of aerodynamic uncertainties. Liu et al. [10] presented an output feedback controller by means of the immersion and invariance technique to provide asymptotically stable estimates of the unmeasurable states. However, it is notable that the control schemes in [8-10] do not fully consider the input nonlinearities of input saturation and dead-zone simultaneously.

From a practical viewpoint, the aerodynamic control surfaces of AHVs are always subject to input saturation [11] and dead-zone [12] due to their physical properties. These two inevitable constraints, as dominant input nonlinearities, often limit system performance severely, and may result in undesirable inaccuracy or lead to instability. With this in mind, the control design of AHVs with explicit consideration of these input nonlinearities has attracted a great interest over the past years. Xu et al. [13] proposed fault-tolerant control algorithms for tracking control of AHVs, in which command filters were introduced to deal with input saturation issue. Almost simultaneously, a similar result was presented in [14]. Later, inspired by [15], an auxiliary system was constructed in [16] to systematically account for the non-symmetric input saturation constraint. Recently, Bu et al. [17] developed a novel auxiliary system which was integrated in the adaptive neural control scheme to handle the physical constraint on actuator. Zhou et al. [18] introduced a mean-value theorem to overcome the obstacle generated from input saturation by combining adaptive backstepping control method. Regarding the dead-zone issue, Xu [19] incorporated the Nussbaum gain into the robust adaptive neural control to account for dead-zone nonlinearity. Despite the recent progress, it is noticed that most of the aforementioned works are focused on either input saturation or dead-zone separately. Actually, these two kinds of input nonlinearities always occur simultaneously, which poses significant challenges for the control design of AHVs. At present, some researches on integrating dead-zone with saturation have been presented in [20-22] for the nonlinear systems, under the assumption that the parameters of dead-zone are known. Yet, this

assumption is not always satisfied in practice, thus making these control schemes not applicable to our work. In view of this, it is necessary to further explore new methodologies for the control design of AHVs with dead-zone and saturation nonlinearities. On the other hand, due to the characteristics of the AHVs, the dynamic model is also subject to aerodynamic uncertainties [23, 24] and flexible modes [25] in practice, which may lead to control performance degradation. Hence, the development of tracking control schemes that are not only robust against aerodynamic uncertainties and flexible modes, but also able to handle input saturation and dead-zone nonlinearities is an imperative to achieve high precision tracking control of AHVs.

Motivated by the above observation, an adaptive control scheme is proposed for AHVs in the presence of input nonlinearities, aerodynamic uncertainties and flexible modes. Specifically, by viewing aerodynamic uncertainties and flexible modes integrally as lumped disturbances, an adaptive backstepping controller and a dynamic inverse controller are designed for the altitude subsystem and the velocity subsystem, respectively. Then, nonlinear disturbance observers (NDO) separated from the controllers design are constructed for each subsystem to estimate the lumped disturbances. Aiming at the altitude subsystem, dynamic surface control (DSC) technique is introduced to eliminate the problem of “explosion of terms” inherent in traditional backstepping approaches, which greatly reduces the computational burden and simplifies the controller structure. Moreover, a modified smooth inverse structure is proposed to compensate the dead-zone effects. By employing this smooth inverse, only slopes of dead-zone are required to be estimated, thus leading to a reduction of the computational burden. An input nonlinear pre-compensator is constructed to handle input saturation and dead-zone nonlinearities, which significantly simplifies the control design for the altitude subsystem. Based on this pre-compensator, an auxiliary system is designed to address the input saturation issue.

The rest of this paper is organized as follows. Section II presents the vehicle model, while Section III presents an input nonlinear pre-compensator for the input nonlinearities. The derivation of the control scheme is presented in Section IV. Then, the closed-loop stability analysis is given in Section V and followed by Section VI in which numerical simulations are performed to validate the effectiveness of the proposed control scheme. Finally, this paper is concluded in Section VII.

II. Model Description

A. Vehicle Model

The flexible model of the longitudinal dynamics of AHVs used in this study is developed by Fiorentini

et al. [25], and can be formulated as

$$\begin{cases} \dot{V} = \frac{T \cos \alpha - D}{m} - g \sin \gamma \\ \dot{h} = V \sin \gamma \\ \dot{\gamma} = \frac{L + T \sin \alpha}{mV} - \frac{g \cos \gamma}{V} \\ \dot{\alpha} = Q - \dot{\gamma} \\ \dot{Q} = \frac{M}{I_{yy}} \\ \ddot{\eta}_i = -2\xi_i \omega_i \dot{\eta}_i - \omega_i^2 \eta_i + N_i, \quad i = 1, 2, 3 \end{cases} \quad (1)$$

where ξ_i and ω_i denote damping ratio and natural frequency for the flexible states η_i , respectively, and m is the vehicle mass. This model is composed of five rigid-body state variables V , h , γ , α , Q which represent velocity, altitude, flight path angle (FPA), angle of attack (AOA), and pitch rate respectively, and six flexible states $\eta = [\eta_1, \dot{\eta}_1, \eta_2, \dot{\eta}_2, \eta_3, \dot{\eta}_3]^T$ corresponding to the first three bending modes of the fuselage. To cancel the lift generated by the elevator deflection, a canard is added to be ganged with the elevator by choosing $\delta_c = k_{ec} \delta_e$, where δ_e denotes the elevator deflection, δ_c denotes the canard deflection, and k_{ec} represents the interconnection gain between the elevator deflection and the canard deflection, i.e., $k_{ec} = -C_L^{\delta_e} / C_L^{\delta_c}$. Therefore, the control inputs are selected as $u = [\phi, \delta_e]^T$, where ϕ represents the fuel equivalence ratio. The outputs to be controlled are selected as $y = [V, h]^T$.

To facilitate the control design, a simplified model has been derived in [26] for control design and analysis, which retains the relevant dynamic characteristics of the simulation model. The approximations of lift, drag, thrust, pitching moment, and generalized forces are given as follows:

$$\begin{cases} T \approx \bar{q} S [C_{T,\phi}(\alpha)\phi + C_T(\alpha) + C_T^\eta \eta] \\ L \approx \bar{q} S C_L(\alpha, \delta, \eta) \\ D \approx \bar{q} S C_D(\alpha, \delta, \eta) \\ M \approx z_T T + \bar{q} S \bar{c} C_M(\alpha, \delta, \eta) \\ N_i \approx \bar{q} S [N_i^{\alpha^2} \alpha^2 + N_i^\alpha \alpha + N_i^{\delta_e} \delta_e + N_i^{\delta_c} \delta_c + N_i^0 + N_i^\eta \eta] \end{cases} \quad (2)$$

where $\delta = [\delta_c, \delta_e]^T$, and \bar{q} , S and \bar{c} represent the dynamic pressure, the reference area, and the reference length, respectively. The coefficients are obtained using curve-fitted approximations, which are presented as

$$\begin{cases}
C_{T,\phi}(\alpha) = C_T^{\phi\alpha^3} \alpha^3 + C_T^{\phi\alpha^2} \alpha^2 + C_T^{\phi\alpha} \alpha + C_T^0 \\
C_T(\alpha) = C_T^3 \alpha^3 + C_T^2 \alpha^2 + C_T^1 \alpha^1 + C_T^0 \\
C_M(\alpha, \delta, \eta) = C_M^{\alpha^2} \alpha^2 + C_M^\alpha \alpha + C_M^{\delta_e} \delta_e + C_M^{\delta_c} \delta_c + C_M^0 + C_M^\eta \eta \\
C_L(\alpha, \delta, \eta) = C_L^\alpha \alpha + C_L^{\delta_e} \delta_e + C_L^{\delta_c} \delta_c + C_L^0 + C_L^\eta \eta \\
C_D(\alpha, \delta, \eta) = C_D^{\alpha^2} \alpha^2 + C_D^\alpha \alpha + C_D^{\delta_e^2} \delta_e^2 + C_D^{\delta_e} \delta_e + C_D^{\delta_c^2} \delta_c^2 + C_D^{\delta_c} \delta_c + C_D^0 + C_D^\eta \eta \\
C_j^\eta = [C_j^{\eta_1} \quad 0 \quad C_j^{\eta_2} \quad 0 \quad C_j^{\eta_3} \quad 0], \quad j = T, M, L, D \\
N_i^\eta = [N_i^{\eta_1} \quad 0 \quad N_i^{\eta_2} \quad 0 \quad N_i^{\eta_3} \quad 0], \quad i = 1, 2, 3
\end{cases} \quad (3)$$

In contrast to [26], the lift, drag, thrust, and moment coefficients presented above depend explicitly on the flexible modes. To facilitate the design, the dynamic equations of the AHVs are transformed into a strict feedback form. Without loss of generality, the aerodynamic uncertainties and flexible modes are regarded as lumped disturbances. As a result, the strict feedback equations are expressed as

$$\begin{aligned}
\dot{V} &= f_V + g_V \phi + d_V \\
\dot{h} &= V \sin \gamma \\
\dot{\gamma} &= f_\gamma + g_\gamma \alpha + d_\gamma \\
\dot{\alpha} &= Q - (f_\gamma + g_\gamma \alpha + d_\gamma) \\
\dot{Q} &= f_Q + g_Q \delta_e + d_Q
\end{aligned} \quad (4)$$

where

$$\begin{cases}
f_V = [qSC_T(\alpha) \cos \alpha - qSC_D(\alpha, \delta)] / m - g \sin \gamma \\
g_V = [qSC_{T,\phi}(\alpha) \cos \alpha] / m \\
f_\gamma = [qSC_L^0 + qS(C_{T,\phi}(\alpha)\phi + C_T(\alpha)) \sin \alpha] / (mV) - g \sin \gamma / V \\
g_\gamma = qSC_L^\alpha / (mV) \\
f_Q = [z_T qS(C_{T,\phi}(\alpha)\phi + C_T(\alpha)) + qS\bar{C}(C_M^{\alpha^2} \alpha^2 + C_M^\alpha \alpha + C_M^0)] / I_{yy} \\
g_Q = qS\bar{C}(C_M^{\delta_e} + k_{ec} C_M^{\delta_c}) / I_{yy}
\end{cases} \quad (5)$$

and d_V , d_Q and d_γ are lumped disturbances including aerodynamic uncertainties and flexible modes.

B. Input Nonlinearities

In this paper, input nonlinearity $\delta_e(v)$ encompasses non-symmetric saturation and dead-zone. That is, the control signal v is constrained by the saturation values $\delta_{e_{\max}}$ and $\delta_{e_{\min}}$, and the dead-zone values b_r and b_l , as shown in Fig. 1. In view of Fig. 1, the input nonlinearity $\delta_e(v)$ can be expressed as

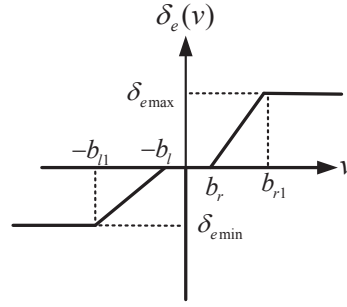


Fig. 1 Non-symmetric saturation and dead-zone model

$$\delta_e(v) = \begin{cases} \chi(t)(v(t) + b_l), & v \leq -b_l \\ \chi(t)(v(t) - b_r), & v > b_r \\ 0, & -b_l < v < b_r \end{cases} \quad (6)$$

in which

$$\chi(t) = \begin{cases} \frac{\delta_{e\min}}{v(t) + b_l}, & v(t) < -b_{l1} \\ m_l, & -b_{l1} \leq v(t) \leq -b_l \\ m_r, & b_r \leq v(t) \leq b_{r1} \\ \frac{\delta_{e\max}}{v(t) - b_r}, & v(t) > b_{r1} \end{cases}$$

where b_l , b_{l1} , b_r , b_{r1} , m_l and m_r are unknown positive constants. It should be pointed out that neither the break-points b_l and b_r nor the slopes m_l and m_r are required to be equal. The parameters $\delta_{e\max}$ and $\delta_{e\min}$ represent the maximum and the minimum allowable elevator deflection angles, respectively.

To facilitate the control law derivation and stability analysis, the following assumptions are made.

Assumption 1 [9], [27]: The functions g_i and f_i ($i = V, \gamma, Q$) are bounded, and there exist positive known constants \bar{g}_i and \bar{f}_i satisfying $\bar{g}_i \geq |g_i| > 0$ and $\bar{f}_i \geq |f_i| > 0$.

Assumption 2: The lumped disturbances are slowly time-varying, and there exist small positive constants M_{d_i} , $i = V, \gamma, Q$, which satisfy $|\dot{d}_i| < M_{d_i}$.

Assumption 3: The parameters m_l and m_r satisfy $\bar{m}_l > m_l > \underline{m}_l$ and $\bar{m}_r > m_r > \underline{m}_r$ respectively, where \underline{m}_l , \underline{m}_r , \bar{m}_r and \bar{m}_l are known positive constants. In addition, b_l and b_r are bounded positive constants.

Lemma 1 [28]: For any variable s and constant $b > 0$, the following inequality always holds $0 \leq |s| - s \tanh(s/b) \leq \nu b$, where $\nu = 0.2758$.

III. Input Nonlinear Pre-Compensator Design

According to the definition of input nonlinearities in (6), the nonlinear characteristics of the actuator are relatively complex and are difficult to directly deal with. With this in mind, in this section, an input nonlinear pre-compensator will be constructed to address these nonlinearities issue, as shown in Fig. 2.

Remark 1: The constraint values, i.e., $\delta_{p\min}$ and $\delta_{p\max}$, in the pre-compensator structure are associated with the unknown slopes m_l and m_r . Thus, these values are not selected equally with $\delta_{e\min}$ and $\delta_{e\max}$. The selection of $\delta_{p\min}$ and $\delta_{p\max}$ will be illustrated in the subsequent analysis, and the inverse structure of dead-zone will also be presented.

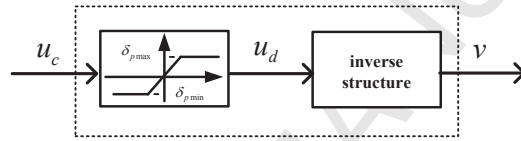


Fig. 2 Input nonlinear pre-compensator structure

By simple transformation, the actual control input $\delta_e(v)$ can be depicted as

$$\delta_e(v) = a(t)v(t) + d(t) \quad (7)$$

where

$$a(t) = \begin{cases} m_l & v(t) \leq 0 \\ m_r & v(t) > 0 \end{cases} \quad (8)$$

and

$$d(t) = \begin{cases} m_l b_l & v(t) \leq -b_l \\ -a(t)v(t) & -b_l < v(t) < b_r \\ -m_r b_r & v(t) \geq b_r \end{cases} \quad (9)$$

Invoking Assumption 3, it is easy to deduce that $d(t)$ is bounded. To facilitate the subsequent control design, we define a new variable, i.e., $u(t) = a(t)v(t)$, which can be further described as

$$u(t) = \begin{cases} m_l v(t) & v(t) \leq 0 \\ m_r v(t) & v(t) > 0 \end{cases} \quad (10)$$

Inspired by [29], the smooth inverse structure of $u(t)$ can be proposed as follows:

$$v(t) = I(u(t)) = \frac{u(t)}{m_l} \varphi_l(u) + \frac{u(t)}{m_r} \varphi_r(u) \quad (11)$$

where φ_l and φ_r are smooth continuous functions defined as

$$\varphi_l(u) = \frac{e^{-u(t)/e_0}}{e^{u(t)/e_0} + e^{-u(t)/e_0}}, \quad \varphi_r(u) = \frac{e^{u(t)/e_0}}{e^{u(t)/e_0} + e^{-u(t)/e_0}}$$

where $e_0 > 0$ is a free design parameter chosen by designers. Further, to estimate the unknown parameters, we parameterize $u(t)$ as

$$u(t) = \varpi^T(t)\theta \quad (12)$$

where $\theta = [m_l, m_r]^T$, and $\varpi = [\sigma_l(v)v(t), \sigma_r(v)v(t)]^T$ with

$$\sigma_l = \begin{cases} 1 & v < 0 \\ 0 & \text{otherwise} \end{cases}, \quad \sigma_r = \begin{cases} 1 & v > 0 \\ 0 & \text{otherwise} \end{cases}$$

As θ is unknown and ϖ is unavailable, we define an auxiliary control input $u_d(t)$ as

$$u_d(t) = \hat{\varpi}^T(t)\hat{\theta} \quad (13)$$

where $\hat{\theta}$ denotes estimation of θ , i.e.,

$$\begin{cases} \hat{\theta} = [\hat{m}_l, \hat{m}_r]^T \\ \hat{\varpi} = [\varphi_l(v(t))v(t), \varphi_r(v(t))v(t)]^T \end{cases} \quad (14)$$

Remark 2: The key idea of compensating dead-zone effects is to employ a smooth dead-zone inverse, and then design adaptive controllers to estimate the unknown parameters, i.e., m_l , $m_l b_l$, m_r and $m_r b_r$, as shown in [29, 30]. However, in contrast to these existing methods, only m_l and m_r are required to be estimated, thus significantly reducing the computational burden.

Then, the corresponding control input $v(t)$ is given by

$$v(t) = I(u_d(t)) = \frac{u_d(t)}{\hat{m}_l} \varphi_l(u_d) + \frac{u_d(t)}{\hat{m}_r} \varphi_r(u_d) \quad (15)$$

The resulting error between u and u_d is

$$u(t) - u_d(t) = \varpi^T(t)\theta - \hat{\varpi}^T(t)\hat{\theta} \quad (16)$$

Through straightforward and equivalent derivation, we obtain

$$u(t) - u_d(t) = \hat{\varpi}^T(t)(\theta - \hat{\theta}) + d_n(t) \quad (17)$$

where $d_n(t) = (\varpi^T(t) - \hat{\varpi}^T(t))\theta$. In view of (12) and (13), the bound of $d_n(t)$ can be obtained as

$$|d_n(t)| \leq \begin{cases} \frac{1}{2}e_0e^{-1}|m_r - m_l|, & v(t) \geq b_r \\ \max\{m_l b_l, m_r b_r, m_r b_l, m_l b_r\}, & -b_l < v(t) < b_r \\ \frac{1}{2}e_0e^{-1}|m_r - m_l|, & v(t) < -b_l \end{cases} \quad (18)$$

where we have used that $|v|e^{-|v|} \leq e^{-1}$. Note that the upper bound of $d_n(t)$ is a function with respect to the parameters of dead-zone. Based on the preceding manipulation, the actual control input $\delta_e(v)$ can be presented as

$$\delta_e(v) = u_d + \hat{\omega}^T(t)\tilde{\theta} + d_N \quad (19)$$

where $d_N = d_n(t) + d(t)$, and $\tilde{\theta} = \theta - \hat{\theta}$. From (7) and (18), there exists a positive constant D such that $|d_N| \leq D$.

Remark 3: As shown in Fig. 2, $u_c(t)$ denotes the nominal control input to be designed for the altitude subsystem. The auxiliary control input $u_d(t)$ is obtained by limiting the magnitude of $u_c(t)$, thus guaranteeing that the actual control input $\delta_e(v)$ always satisfies the saturation constraint. Then, the modified smooth inverse is employed to convert $u_d(t)$ to the control input $v(t)$ for the purpose of compensating the dead-zone effects. Additionally, the new variable $u(t)$ introduced in this section is only used to analyze the modified smooth inverse.

Remark 4: Apart from u_d , the remaining terms on the right-hand side of (19) are obviously unknown, which makes the selection of constraint values, i.e., $\delta_{p\min}$ and $\delta_{p\max}$, in pre-compensator structure a challenging problem. Given this, the detailed procedure for selecting these constraint values is presented as follows according to (7) and (15). Regarding the case of $v(t) > 0$, by simple computing, it can be obtained that the inequality $\delta_e(t) \leq a(t)v(t)$ always holds, which is pivotal for the subsequent analysis. Invoking Assumption 3, the upper bound of $v(t)$ can be chosen as $\delta_{e\max}/\bar{m}_r$. Then, according to (15), the maximum of $\delta_{p\max}$ can be selected as $\delta_{e\max}m_r/\bar{m}_r$ to guarantee that $v(t)$ complies with constraint $v(t) \leq \delta_{e\max}/\bar{m}_r$, thereby meeting the saturation constraint of the actual input $\delta_e(v)$. Note that the selection procedure for the case of $v(t) \leq 0$ is similar with the above discussion, thus it is omitted here.

IV. Nonlinear Controller Design

The starting point is to divide the vehicle model into two functional subsystems, i.e., velocity

subsystem and altitude subsystem for (4). Then, the corresponding controllers are elaborately designed for these two subsystems. More specifically, the DSC technique is employed for the altitude subsystem subject to dead-zone and input saturation. Applying the nonlinear dynamic inversion technique, a robust controller is designed for the velocity subsystem.

A. Controller Design for the Velocity Subsystem

According to (4), the dynamics of velocity tracking error, i.e. $\tilde{V} = V - V_{ref}$, can be calculated as

$$\dot{\tilde{V}} = f_V + g_V \phi + d_V - \dot{V}_{ref} \quad (20)$$

where V_{ref} is the reference signal possessing a bounded first-order derivative. To dispose of the lumped disturbance d_V , an NDO is constructed as

$$\begin{cases} \dot{p}_V = -l_V p_V - l_V (\lambda_V + f_V + g_V \phi) \\ \hat{d}_V = p_V + \lambda_V \end{cases} \quad (21)$$

where \hat{d}_V is the estimation of d_V and l_V is the NDO gain, which is determined by $l_V = \frac{\partial \lambda_V}{\partial V}$.

Defining the estimation error as $e_V = d_V - \hat{d}_V$, the time derivative of e_V is computed as

$$\dot{e}_V = -l_V e_V + \dot{d}_V \quad (22)$$

To simplify the design procedure, we borrow a conclusion from [31] without proof, that is, the estimation error e_V is bounded, and it is bounded by M_{d_V}/l_V . In practical terms, due to the physical limitation, the engine could not always provide sufficient thrust to maintain the favorable tracking performance when the control input becomes saturated. To address this issue, we introduce an auxiliary system to generate certain compensating signal for weakening the negative effects caused by saturation constraint. The auxiliary system can be described as [32]

$$\dot{\chi}_V = -k_\chi \chi_V + g_V (\phi - \phi_c) \quad (23)$$

where ϕ_c is the nominal control law and k_χ is a positive definite design parameter. Defining

$z_V = \tilde{V} - \chi_V$ as the modified velocity tracking error, the derivative of z_V can be calculated as

$$\dot{z}_V = f_V + g_V \phi_c + d_V - \dot{V}_{ref} + k_\chi \chi_V \quad (24)$$

Consider a quadratic form

$$\Gamma_V = \frac{1}{2} z_V^2 \quad (25)$$

Its derivative is given by

$$\dot{\Gamma}_V = z_V (f_V + g_V \phi_c + d_V - \dot{V}_{ref} + k_\chi \chi_V) \quad (26)$$

In accordance with (22)-(24), by applying nonlinear dynamic inversion technique, the nominal control input ϕ_c is designed as

$$\phi_c = g_V^{-1} (-k_V z_V - f_V - \hat{d}_V + \dot{V}_{ref} - k_\chi \chi_V) \quad (27)$$

Note that the value of g_V is nonzero owing to Assumption 1. Substituting (27) into (26), we can obtain

$$\dot{\Gamma}_V = -k_V z_V + z_V e_V \quad (28)$$

where k_V is a positive gain parameter.

B. Controller Design for the Altitude Subsystem

From (4), the altitude tracking error is defined as

$$\tilde{h} = h - h_{ref} \quad (29)$$

where h_{ref} is the reference signal, which has the bounded derivative. For the cruising phase, the flight path angle γ is close to zero, which implies $\sin \gamma \approx \gamma$. Given this, the flight path angle command can be selected as

$$\gamma_d = \frac{-k_h \tilde{h} + \dot{h}_r}{V} \quad (30)$$

where k_h is a positive constant. If the flight path angle γ accurately tracks the desired reference signal γ_d , then it follows from (29) and (30) that

$$\dot{\tilde{h}} = -k_h \tilde{h} \quad (31)$$

which apparently guarantees that \tilde{h} converges to zero. Therefore, the altitude subsystem controller can be designed to steer γ to track the desired reference signal γ_d to accomplish the altitude tracking mission.

Step 1: In the beginning, the dynamics of the FPA tracking error can be expressed as

$$\dot{\tilde{\gamma}} = \gamma - \gamma_d \quad (32)$$

Recalling (4), the first-order derivative of the tracking error is computed as

$$\dot{\tilde{\gamma}} = f_\gamma + g_\gamma \alpha + d_\gamma - \dot{\gamma}_d \quad (33)$$

To ensure the completion of the following control design, another NDO is designed, similar to (21), to

estimate the lumped disturbance d_γ . In view of the conclusion in [31], the estimation error i.e., $e_\gamma = d_\gamma - \hat{d}_\gamma$, is bounded by M_{d_γ} / l_γ , where \hat{d}_γ is the estimation of d_γ and l_γ denotes the NDO gain. Since the function of g_γ is nonzero according to Assumption 1, to derive $\tilde{\gamma} \rightarrow 0$, the following virtual control signal is chosen as:

$$\alpha_c = g_\gamma^{-1}(-k_\gamma \tilde{\gamma} - f_\gamma - \hat{d}_\gamma + \dot{\gamma}_d) \quad (34)$$

Obviously, the derivative of the virtual control signal will become increasingly complicated as the system order increases. To remedy this, we introduce the dynamic surface control [33], capable of eliminating the problem of “explosion of terms” inherent in backstepping control. Let the virtual control signal, i.e., α_c , pass through a first-order filter to generate α_d and its derivative $\dot{\alpha}_d$ as

$$\tau_\alpha \dot{\alpha}_d + \alpha_d = \alpha_c \quad (35)$$

Next, the dynamics of the FPA tracking error $\tilde{\gamma}$ can be further calculated as

$$\dot{\tilde{\gamma}} = -k_\gamma \tilde{\gamma} + e_\gamma + g_\gamma y_\alpha + \tilde{\alpha} \quad (36)$$

where $\tilde{\alpha}$ is AOA tracking error described as $\tilde{\alpha} = \alpha - \alpha_d$, y_α represents the virtual variable estimation error defined as $y_\alpha = \alpha_d - \alpha_c$, and k_γ denotes the control gain for the FPA tracking error. Choose a quadratic form as

$$L_\gamma = \frac{1}{2} \tilde{\gamma}^2 + \frac{1}{2} y_\alpha^2 \quad (37)$$

Differentiating L_γ with respect to time and substituting (33) and (34) result in

$$\dot{L}_\gamma = -k_\gamma \tilde{\gamma}^2 + \tilde{\gamma} e_\gamma + \tilde{\gamma} g_\gamma y_\alpha + \tilde{\gamma} \tilde{\alpha} + y_\alpha (\dot{\alpha}_d - \dot{\alpha}_c) \quad (38)$$

Step 2: By simple calculation, we can get the time derivative of the AOA tracking error as

$$\dot{\tilde{\alpha}} = Q - (f_\gamma + g_\gamma \alpha + d_\gamma) - \dot{\alpha}_d \quad (39)$$

The estimation of d_γ is expressed as \hat{d}_γ , which has been derived in Step 1. Similarly, the virtual control law Q_c can be designed as

$$Q_c = -k_\alpha \tilde{\alpha} + (f_\gamma + g_\gamma \alpha + \hat{d}_\gamma) + \dot{\alpha}_d - \chi_{u_c} \quad (40)$$

where χ_{u_c} will be defined at a later stage. Then, applying DSC technique, the estimation of Q_c can be derived from

$$\tau_Q \dot{Q}_d + Q_d = Q_c \quad (41)$$

where Q_d is the estimation of Q_c and τ_Q denotes the time constant. As a consequence, the time derivative of the AOA tracking error can be rewritten as

$$\dot{\tilde{\alpha}} = -k_\alpha \tilde{\alpha} - e_\gamma + z_u + y_Q \quad (42)$$

where $y_Q = Q_d - Q_c$, k_α is constant parameter to be designed later, and z_u will be defined at the next step. Define a quadratic form as

$$L_\alpha = \frac{1}{2} \tilde{\alpha}^2 + \frac{1}{2} y_Q^2 \quad (43)$$

Taking the time derivative of L_α and substituting (42) yield

$$\dot{L}_\alpha = -k_\alpha \tilde{\alpha}^2 - \tilde{\alpha} e_\gamma + \tilde{\alpha} z_u + y_Q (\dot{Q}_d - \dot{Q}_c) \quad (44)$$

Step 3: The first-order derivative of \tilde{Q} can be computed as

$$\dot{\tilde{Q}} = f_Q + g_Q \delta_e(v) + d_Q - \dot{Q}_d \quad (45)$$

Recalling the expression of $\delta_e(v)$ in (19), equation (45) can be rewritten as

$$\dot{\tilde{Q}} = f_Q + g_Q u_d + g_Q \hat{w}^T(t) \tilde{\theta} + g_Q d_N + d_Q - \dot{Q}_d \quad (46)$$

To handle input saturation, another auxiliary system is constructed as follows:

$$\dot{\chi}_{u_c} = -k_{\chi_{u_c}} \chi_{u_c} + g_Q (u_d - u_c) \quad (47)$$

where χ_{u_c} is the state of the auxiliary system, and u_c is the nominal control input. Similarly, the estimation of d_Q can be derived by constructing a relevant NDO and the estimation error i.e., e_Q is bounded by M_{d_Q} / l_Q . Combining (46) and (47), the modified error, i.e., $z_u = Q - Q_d - \chi_{u_c}$, satisfies

$$\dot{z}_u = f_Q + g_Q u_c + g_Q d_N + g_Q \hat{w}^T \tilde{\theta} + d_Q - \dot{Q}_d + k_{\chi_{u_c}} \chi_{u_c} \quad (48)$$

Finally, the nominal control input is designed as

$$u_c = g_Q^{-1} [-k_Q z_u - k_{\chi_{u_c}} \chi_{u_c} - f_Q - g_Q \hat{D} \tanh(\frac{g_Q \tilde{Q}}{\varsigma}) - \hat{d}_Q + \dot{Q}_d] \quad (49)$$

where \hat{D} is the estimation of D and k_Q is a positive constant. Notice that g_Q is nonzero in the cruising phase. For the uncertain parameters D and θ , the adaptive laws are chosen as

$$\begin{cases} \dot{\hat{D}} = \Gamma_D^{-1} g_Q z_u \tanh(\frac{g_Q z_u}{\varsigma}) - \Gamma_D^{-1} l_D (\hat{D} - D_0) \\ \dot{\hat{\theta}} = \text{Proj}[\Gamma_\theta^{-1} g_Q \hat{w}^T z_u - \Gamma_\theta^{-1} l_\theta (\hat{\theta} - \theta_0)] \end{cases} \quad (50)$$

where Γ_D , l_D , Γ_θ and l_θ are positive constants, which are designed by projectors later. D_0 and θ_0 are also design parameters, which can be chosen to be zero when one does not obtain precisely prior knowledge on them. $\text{Proj}(\cdot)$ in (50) denotes the projection operator that is used here to modulate the estimations within the admissible ranges. The projection has the following form:

$$\text{Proj}(\zeta) = \begin{cases} 0, & \text{if } \hat{p}_i = p_i^l, \zeta \leq 0, \\ \hat{p}_i = p_i^u & \zeta \geq 0 \\ \zeta, & \text{otherwise} \end{cases} \quad (51)$$

Define a quadratic form as

$$L_Q = \frac{1}{2} z_u^2 + \frac{1}{2} \Gamma_\theta \tilde{\theta}^T \tilde{\theta} + \frac{1}{2} \Gamma_D \tilde{D}^2 \quad (52)$$

where $\tilde{\theta} = \theta - \hat{\theta}$ and $\tilde{D} = D - \hat{D}$. From (48)-(50) and (52), the first-order derivative of L_Q can be calculated as

$$\dot{L}_Q \leq -k_Q z_u^2 - z_u e_Q - z_u g_Q \hat{D} \tanh\left(\frac{g_Q z_u}{\zeta}\right) + l_\theta \tilde{\theta}^T (\hat{\theta} - \theta) + z_u g_Q d_N - \Gamma_D \tilde{D} \dot{\tilde{D}} \quad (53)$$

Remark 5: At the above steps, the first-order filters are introduced to filter virtual control signals x_c ($x = \alpha, Q$) and obtain x_d as well as \dot{x}_d . Then x_d and \dot{x}_d are used to replace x_c and \dot{x}_c at the next step, respectively. As a result, the explosion of complexity problem is successfully avoided and the controller constructed is significantly simplified.

Remark 6: By constructing the input nonlinear pre-compensator illustrated in Fig. 2, the input saturation can be dealt with through some common control approaches used for saturated systems, thus enhancing the flexibility in accounting for input nonlinearities and simplifying the control design.

V. Stability Analysis

The goal pursued in this section is to evaluate the stability properties of the resulting closed-loop system. To investigate system stability, we begin with introducing the following Lyapunov candidate function for the overall system:

$$L = \Gamma_V + L_Y + L_\alpha + L_Q \quad (54)$$

Differentiating L and using (28), (38), (44) and (53) lead to

$$\begin{aligned}
\dot{L} \leq & -(k_v - \frac{1}{2})z_v + \frac{1}{2}e_v^2 - k_\gamma \tilde{\gamma}^2 + \tilde{\gamma}e_\gamma + \tilde{\gamma}g_\gamma y_\alpha + \tilde{\gamma}\tilde{\alpha} \\
& + y_\alpha(\dot{\alpha}_d - \dot{\alpha}_c) - k_\alpha \tilde{\alpha}^2 - \tilde{\alpha}e_\gamma + \tilde{\alpha}z_u + y_Q(\dot{Q}_d - \dot{Q}_c) \\
& - k_Q z_u^2 - z_u e_Q - z_u g_Q \hat{D} \tanh(\frac{g_Q z_u}{\varsigma}) + l_\theta \tilde{\theta}^T (\hat{\theta} - \theta) \\
& + z_u g_Q d_N - \Gamma_D \tilde{D} \dot{\tilde{D}}
\end{aligned} \tag{55}$$

As shown in (55), $\dot{\alpha}_c$ and \dot{Q}_c are the derivatives of α_c and Q_c , respectively. By using tedious but straightforward calculations, we can get continuous functions η_α and η_Q such that

$$\begin{cases} \dot{\alpha}_c \leq \eta_\alpha \\ \dot{Q}_c \leq \eta_Q \end{cases} \tag{56}$$

Then, in accordance with the definition of first-order filters, we have

$$\dot{x}_d = -\frac{y_x}{\tau_x} \tag{57}$$

Substituting (56) and (57) into (55) and invoking Lemma 1 yield

$$\begin{aligned}
\dot{L} \leq & -k_v z_v^2 + \Gamma_v e_v - k_\gamma \tilde{\gamma}^2 + \tilde{\gamma}e_\gamma + \tilde{\gamma}g_\gamma y_\alpha + \tilde{\gamma}\tilde{\alpha} + |y_Q| \eta_Q \\
& - k_\alpha \tilde{\alpha}^2 - \tilde{\alpha}e_\gamma + \tilde{\alpha}z_u + \tilde{\alpha}y_Q - k_Q z_u^2 + l_\theta \tilde{\theta}^T (\hat{\theta} - \theta_0) \\
& + l_D \tilde{D} (\hat{D} - D_0) + e_Q z_u - \frac{y_\alpha^2}{\tau_\alpha} - \frac{y_Q^2}{\tau_Q} + |y_\alpha| \eta_\alpha
\end{aligned} \tag{58}$$

For the above consequence, we have the following useful properties:

$$\begin{cases} l_D \tilde{D} (\hat{D} - D_0) \leq -\frac{1}{2} l_D \tilde{D}^2 + \frac{1}{2} l_D (D - D_0)^2 \\ l_\theta \tilde{\theta}^T (\hat{\theta} - \theta_0) \leq -\frac{1}{2} l_\theta \tilde{\theta}^T \tilde{\theta} + \frac{1}{2} l_\theta (\theta - \theta_0)^T (\theta - \theta_0) \end{cases} \tag{59}$$

Employing Young's inequality and incorporating (59) into (58), the derivative of L can be further computed as

$$\begin{aligned}
L \leq & -(k_v - \frac{1}{2})z_v^2 - (k_\gamma - 1 - \frac{\bar{g}_\gamma^2}{2})\tilde{\gamma}^2 - (k_\alpha - 2)\tilde{\alpha}^2 - (k_Q - 1)z_u^2 - y_\alpha^2 (\frac{1}{\tau_\alpha} - \frac{1}{2} - \frac{\eta_\alpha^2}{2\sigma}) \\
& - y_Q^2 (\frac{1}{\tau_Q} - \frac{1}{2} - \frac{\eta_Q^2}{2\sigma}) - \frac{1}{2} \tilde{\theta}^T l_\theta \tilde{\theta} - \frac{1}{2} l_D \tilde{D}^2 + M
\end{aligned} \tag{60}$$

where σ is an arbitrarily small positive constant. M is defined as $M = \frac{1}{2} l_D (D - D_0)^2 +$

$$\frac{1}{2} l_\theta (\theta - \theta_0)^T (\theta - \theta_0) + \sigma + \frac{1}{2} (\frac{M_{d_v}}{l_v})^2 + \frac{1}{2} (\frac{M_{d_Q}}{l_Q})^2 + (\frac{M_{d_\gamma}}{l_\gamma})^2.$$

Theorem 1: Consider the AHV (4) with uncertain lumped disturbances and input nonlinearities

described by (6) satisfying Assumptions 2 and 3. Under the control laws (27) and (49), and parameter updated laws (50), for any bounded initial condition, there exist design parameters k_i , $i = V, \gamma, \alpha, Q$, such that the error variables, i.e., z_v , \tilde{h} , $\tilde{\gamma}$, $\tilde{\alpha}$ and z_u are bounded. Moreover, the output tracking errors z_v and $\tilde{\gamma}$ remain within the compact set Ω defined by

$$\Omega := \{z_v, \tilde{\gamma} \in \mathbb{R} \mid |z_v| \leq \sqrt{E}, |\tilde{\gamma}| \leq \sqrt{E}\}$$

where $E = 2(L(0) + M/\underline{a})$ with \underline{a} defined in (62).

Proof: Consider the set $A := \{z_v^2 + \tilde{\gamma}^2 + \tilde{\alpha}^2 + \tilde{Q}^2 + y_i^2 + \tilde{\theta}^T \Gamma_\theta \tilde{\theta} + \Gamma_D \tilde{D}^2 < 2p, i = \alpha, Q\}$. Note that the set A is a compact set, there exist maximum values of $\eta_x, i = \alpha, Q$ on the set A . These maximum values are denoted as $M_i, i = \alpha, Q$. From the preceding analysis, let $a_0 > 0$, the control parameters involved in the proposed control scheme can be selected as following to guarantee the system stability:

$$\begin{cases} k_V > \frac{1}{2} + \frac{1}{2}a_0, k_\alpha > 2 + \frac{1}{2}a_0 \\ k_Q > 1 + \frac{1}{2}a_0, k_\gamma > 1 + \frac{\bar{g}_\gamma^2}{2} + \frac{1}{2}a_0 \\ \frac{1}{\tau_Q} > \frac{1}{2} + \frac{M_Q}{2\sigma} + \frac{1}{2}a_0 \\ \frac{1}{\tau_\alpha} > \frac{1}{2} + \frac{M_\alpha}{2\sigma} + \frac{1}{2}a_0 \end{cases} \quad (61)$$

Substituting (61) into (60) and rearranging yield

$$\dot{L} \leq -\underline{a_0}L + M \quad (62)$$

where $\underline{a_0} = \min\{a_0, l_\theta/\Gamma_\theta, l_D/\Gamma_D\}$. Let $\underline{a_0} \geq M/p$, it follows that $\dot{L} \leq 0$ on $L = p$. Therefore, $L \leq p$ is an invariant set. Furthermore, integrating (62) and through straightforward calculations, we have

$$L \leq L(0) + \frac{M}{\underline{a_0}} \quad (63)$$

Next, in accordance with (25), (32), (54) and (63), we obtain

$$\begin{cases} \frac{1}{2}z_v^2 \leq L(0) + \frac{M}{\underline{a_0}} \Rightarrow |z_v| \leq \sqrt{2(L(0) + \frac{M}{\underline{a_0}})} \\ \frac{1}{2}\tilde{\gamma}^2 \leq L(0) + \frac{M}{\underline{a_0}} \Rightarrow |\tilde{\gamma}| \leq \sqrt{2(L(0) + \frac{M}{\underline{a_0}})} \end{cases} \quad (64)$$

As a consequence, z_v and $\tilde{\gamma}$ are uniformly ultimately bounded. Meanwhile, the tracking errors can

converge to an arbitrarily small neighborhood around zero with the appropriate choice of the control parameters.

Remark 7: The procedure for choosing the control law gains can be summarized as the following steps:

Step 1: Choose the time constants τ_α and τ_Q according to the equation (61) and they should be chosen small values. The NDO gains, i.e., l_v , l_Q and l_γ , should be set no more than one third of the frequency of the first vibration mode ω_1 to avoid exciting the flexible dynamics.

Step 2: Choose the control law gains k_i $i = V, \alpha, Q, \gamma$, according to the equation (61), while they shouldn't be selected too large due to the bounded control input. Therefore, one should balance the tracking performance and the control input to select appropriate values.

Step 3: The positive parameters Γ_D , l_D , Γ_θ and l_θ should be chosen and modulated in accordance with the magnitude of relevant variables.

VI. Simulation Results

In this section, simulation results are presented to illustrate the effectiveness of the proposed scheme. The initial values of the reference commands are chosen as $V(0) = 7850 \text{ ft/s}$ and $h(0) = 86000 \text{ ft}$, while the final values are taken as $V(\infty) = 9850 \text{ ft/s}$ and $h(\infty) = 96000 \text{ ft}$. The references of V_{ref} and h_{ref} are generated by filtering corresponding step commands with second-order pre-filters, which are chosen with same natural frequency of 0.03 rad/s and same damping factor of 0.95. The initial values of AOA and pitch angle are all set as 3.5° , and elevator deflection and fuel equivalence ratio are chosen as 0. Furthermore, the admissible ranges of states and inputs are illustrated in Table 1.

Table 1. The permissible ranges of states and inputs.

Variable	Min value	Max value
Velocity (ft/s)	7000	10000
Altitude (ft)	80000	120000
AOA (deg)	-6	6
FPA (deg)	-3	3
Pitch rate (deg/s)	-10	10
Elevator deflection (deg)	-20	20
Fuel-to-air ratio	0.05	1.2

The detailed coefficients of the system can be acquired in [25]. Based on the engineering experience,

the dead-zone parameters are chosen as $b_l = 0.02$, $b_r = 0.03$, $m_l = 0.95$, and $m_r = 1.05$, whereas the bounded values of slopes are selected as $\underline{m}_l = \underline{m}_r = 0.9$, and $\bar{m}_l = \bar{m}_r = 1.1$.

To verify the proposed controllers more effectively, simulation results are divided into the following two representative cases:

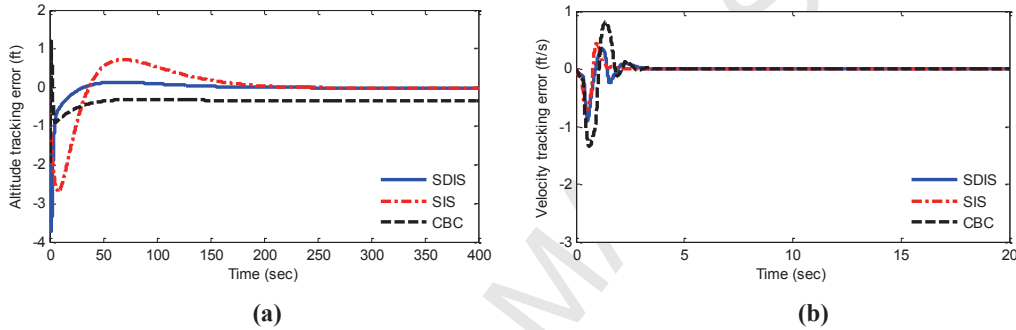
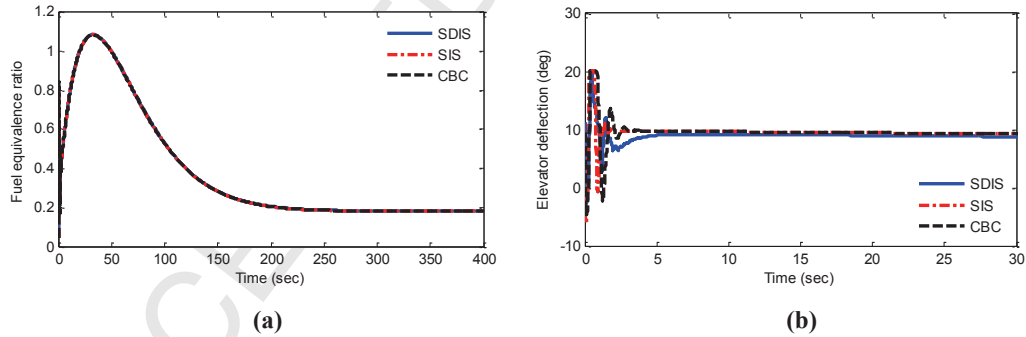
A. Simulation for the AHV Without Input Constraint

Simulation on the longitudinal model of AHVs with no input constraint is presented first to test the good tracking performance of the proposed controller. The performance of the modified smooth inverse structure (noted as SIS) proposed in this paper is compared to the traditional smooth dead-zone inverse structure (noted as SDIS) in [29] and the conventional backstepping control (noted as CBC) scheme without handling the dead-zone. The control parameters used in the subsequent simulations were judiciously selected by trial and error for achieving a good tracking performance. The main control parameters of the three control schemes are presented in Table 2.

Simulation results under the aforementioned three control schemes are presented in Figs. 3 and 4. To be specific, the tracking errors of altitude and velocity are shown in Fig. 3. As shown in Fig. 3(a), it can be seen that the tracking errors of altitude under both SIS and SDIS schemes exhibit a good convergence trend to a small neighborhood around zero in the presence of dead-zone, aerodynamic uncertainties and flexible modes, whereas the tracking error under CBC scheme is unsatisfactory due to the large steady error. Meanwhile, from Fig. 3, it is obvious that the SIS scheme shows better tracking performance in terms of the magnitude of tracking errors when compared to SDIS scheme. Furthermore, as illustrated in Remark 2, there exist fewer uncertain parameters to be estimated under the SIS scheme, which also embodies the superiority of the proposed control scheme. In addition, control inputs under these control schemes are demonstrated in Fig. 4. By inspecting these figures, we may notice that the control inputs δ_e are smooth and bounded, but the upper bound of 20° is exceeded by all algorithms. In view of this, the input constraint should be further explicitly considered during the design procedure.

Table 2. Control parameters for simulation.

Control schemes	Control parameters
Proposed control scheme	$k_V = 3, k_h = 2, k_\gamma = 2.2, k_\alpha = 2.5, k_Q = 3, \tau_i = 0.1, \Gamma_\theta = 5, \Gamma_D = 1, l_\theta = 1, l_D = 1, \theta_0 = [0.9, 1.0]^T, D_0 = 0.01, l_V = 5, l_Q = 5, l_\gamma = 2$
Control scheme in [29]	$k_V = 5, k_h = 2, k_\gamma = 2, k_\alpha = 2, k_Q = 3, \tau_i = 0.1, \Gamma_\theta = 6, \Gamma_D = 1, l_\theta = 1, l_D = 1, \theta_0 = [0.9, 0.01, 1, 0.01]^T, D_0 = 0.02, l_V = 4, l_Q = 6, l_\gamma = 5$
Conventional back-stepping control	$k_V = 3, k_h = 2, k_\gamma = 3, k_\alpha = 3, k_Q = 3, \tau_i = 0.1, l_V = 4, l_Q = 8, l_\gamma = 6$

**Fig. 3 Time responses of tracking errors: (a) Altitude tracking error, (b) Velocity tracking error.****Fig. 4 Time responses of the control inputs: (a) Fuel equivalence ratio, (b) Elevator deflection.**

B. Simulation for the AHV With Input Constraint and Dead-Zone

In this scenario, a severe case in which the actuator of the elevator not only suffers from dead-zone but also input constraint is considered. For comparison, in addition to the proposed controller (noted as SIS), the control scheme employed in [20] is also presented here, in which the input saturation and dead-zone nonlinearities are regarded as an input saturation by applying the right inverse of dead-zone (RIOD). Simulation results under the SIS and the RIOD schemes are illustrated in Figs. 5-13. More specifically,

the tracking responses of altitude and velocity are depicted in Fig. 5, whereas the corresponding tracking errors are demonstrated in Fig. 6. As can be seen from Fig. 6, the SIS scheme exhibits the better tracking performance in terms of the magnitude of tracking errors when compared to the RIOD scheme, although the latter scheme is implemented with the known parameters of dead-zone. Further, to illustrate the tracking performance, a performance index function is introduced and defined as $E = \int_0^t e^2 d\tau$, where t denotes the simulation time and e represents the tracking errors, i.e., \tilde{h} and \tilde{V} . The comparison results are provided in Fig. 8. Obviously, the proposed SIS scheme generates the less error energy compared to the RIOD scheme. The control inputs under the both schemes are plotted in Fig. 7. It is apparent that all control inputs are constrained in the available ranges. By selecting appropriate constraint values according to the Remark 4, the response of the nominal control input u_c is indicated in Fig. 9. Meanwhile, these restrictions, i.e., $\delta_{p_{\min}}$ and $\delta_{p_{\max}}$, guarantee that the elevator deflection always ranges within its bound, as shown in Fig. 7. Moreover, Fig. 11 records other significant states of the AHVs, that is, AOA, FPA, and pitch rate. It can be seen that all these states are within the admissible ranges illustrated in Table 1, and they are almost coincident with corresponding virtual control signals. Estimation results of the NDOs are given in Fig. 12 (d_{r1} , d_{Q1} and $d_{\gamma1}$ denote the estimation of d_r , d_Q and d_γ respectively), while the flexible states are demonstrated in Fig. 10. Additionally, the representative parameters C_L and $C_{T,\phi}$ have been selected separately to implement the aerodynamic parameter perturbation analysis under the SIS scheme. The simulation results are shown in Fig. 13. It is clearly indicated that, in spite of the existing of perturbations, the vehicle still sustains a desirable tracking performance under the proposed control scheme.

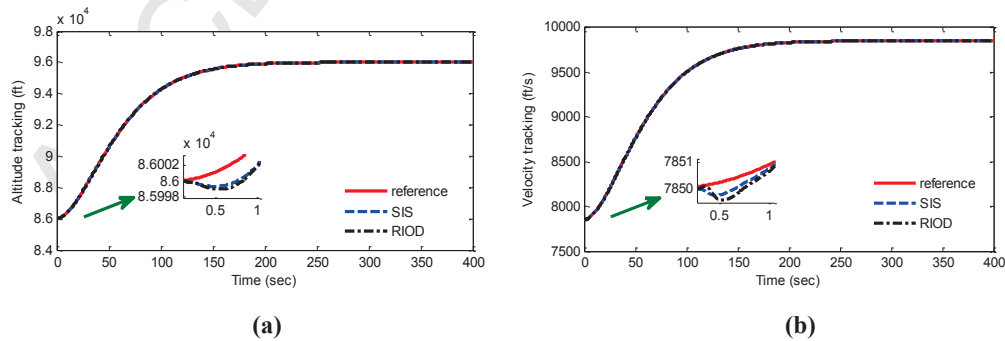


Fig. 5 Tracking responses: (a) Altitude tracking, (b) Velocity tracking.

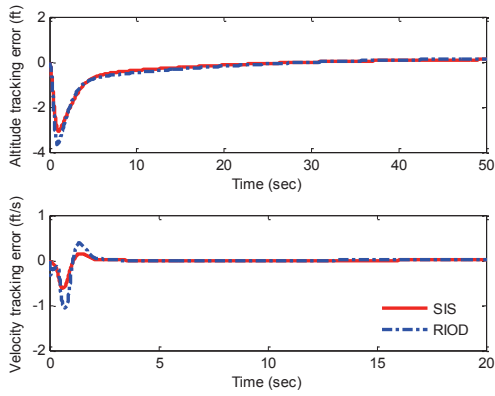


Fig. 6 Time responses of tracking errors.

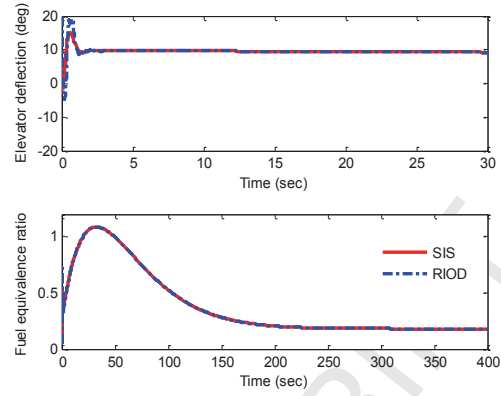
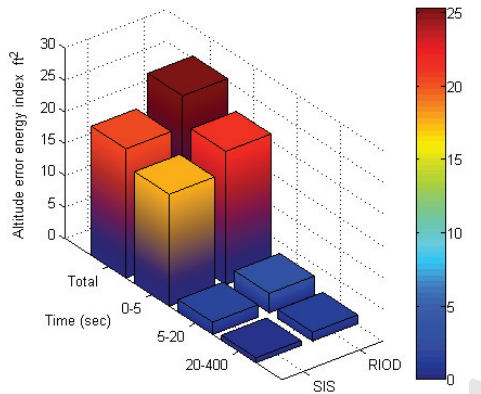
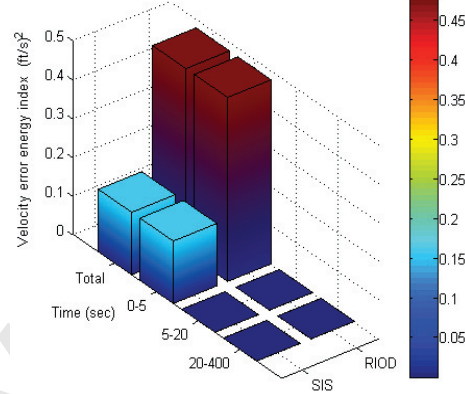


Fig. 7 Time responses of the control inputs.



(a)



(b)

Fig. 8 Error energy: (a) Altitude error energy, (b) Velocity error energy.

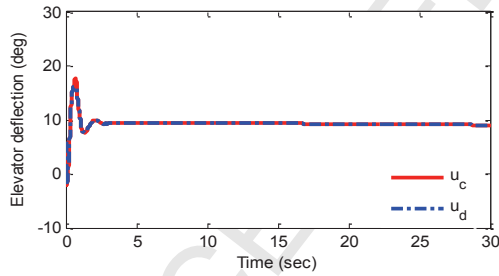
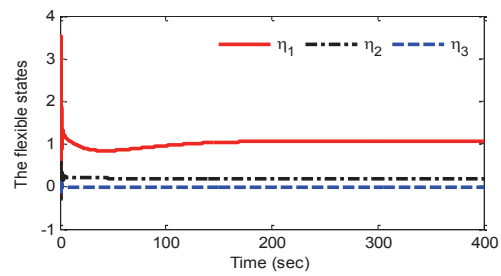
Fig. 9 The response of nominal control input u_c .

Fig. 10 Time responses of the flexible states.

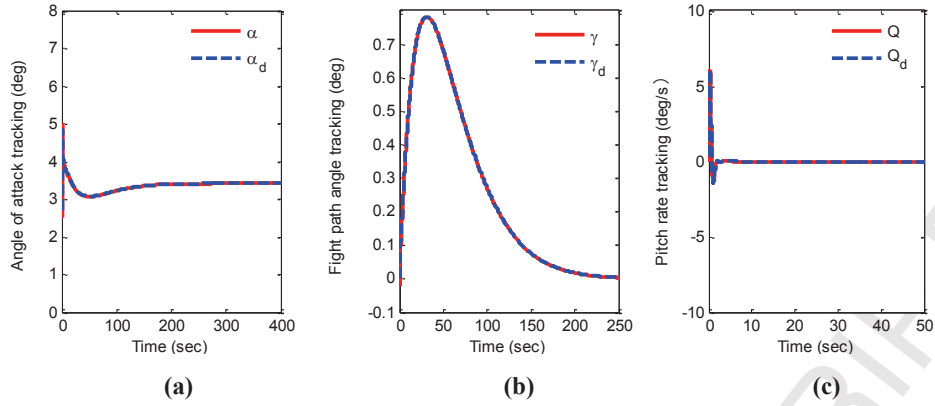


Fig. 11 Time reponses of system states: (a) Angle of attack, (b) Fight path angle, (c) Pitch rate.

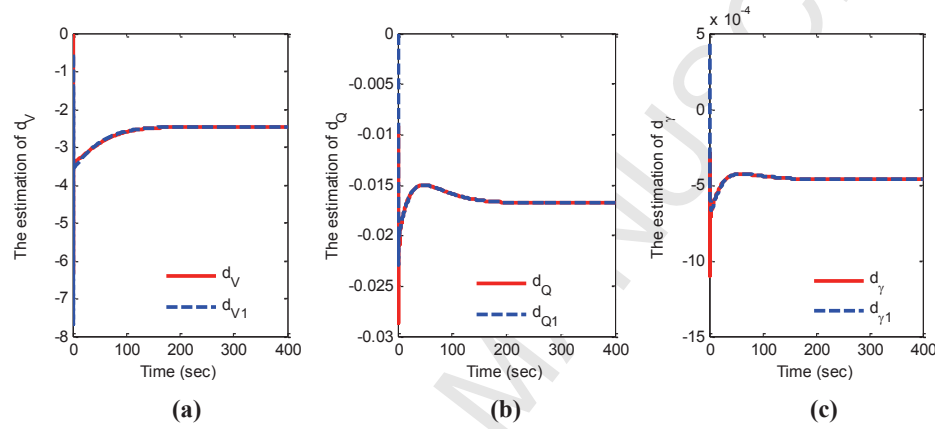


Fig. 12 Results of lumped disturbances estimation: (a) d_V , (b) d_Q , (c) d_γ .

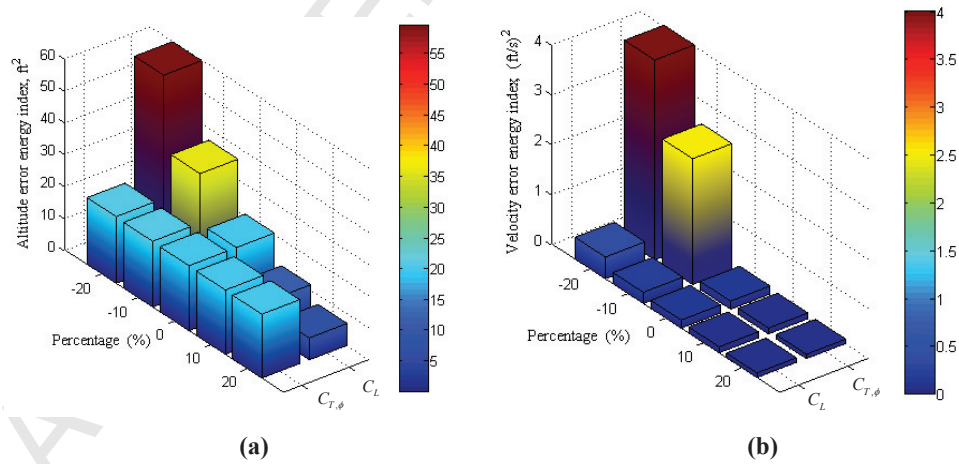


Fig. 13 Aerodynamic parameter perturbation analysis: (a) Altitude error energy, (b) Velocity error energy.

Summarizing all of the simulation cases, it is noticed that the proposed scheme accomplishes the expected mission successfully, despite the presence of input nonlinearities, aerodynamic uncertainties and flexible modes, and shows superior performance compared to other schemes. Moreover, the

flexibility in selecting control parameters can be used to obtain the desired performance while satisfying the constraints on the control magnitude.

VII. Conclusion

This paper has investigated the longitudinal flight control problem of AHVs with input nonlinearities, aerodynamic uncertainties and flexible modes. An adaptive backstepping controller and a dynamic inverse controller have been designed for the altitude subsystem and velocity subsystem, respectively. The proposed dynamic surface control scheme is free of the problem of “explosion of terms”, thus significantly reducing the computational burden. In particular, a modified smooth inverse has been developed in this work. The utilization of this modified inverse not only compensates dead-zone effects but also relieves the computational burden. As another highlight of this paper, an input nonlinear pre-compensator has been proposed to handle input saturation and dead-zone. As such, this pre-compensator also simplifies the control design for the altitude subsystem subject to these two types of input nonlinearities. The simulation results have illustrated the effectiveness of the proposed control scheme. In view of the input nonlinearities, one would focus on the integration of hysteresis and saturation based on the adaptive backstepping control to obtain the preferable control performances in the future work.

ACKNOWLEDGMENT

This work was supported partially by National Natural Science Foundation of China (Project No. 61522301, 61633003). The authors greatly appreciate the above financial support. The authors would also like to thank the associate editor and reviewers for their valuable comments and constructive suggestions that helped to improve the paper significantly.

References

- [1] Schmidt, D. K., “Dynamics and Control of Hypersonic Aeropropulsive/Aeroelastic Vehicles,” *Guidance Navigation and Control Conference*, 1992, pp. 1992-4326.
- [2] Schmidt, D. K., “Optimum Mission Performance and Multivariable Flight Guidance for Airbreathing Launch Vehicles,” *Journal of Guidance, Control, and Dynamics*, Vol. 20, No. 6, 1997, pp. 1157–1164.
- [3] Chavez, F. R., and Schmidt, D. K., “Analytical Aeropropulsive-Aeroelastic Hypersonic-Vehicle Model With Dynamic Analysis,” *Journal of Guidance, Control, and Dynamic*, Vol. 17, No. 6, 1994, pp. 1308-1319.

- [4] Chavez, F. R., and Schmidt, D. K., "Uncertainty Modeling for Multivariable-Control Robustness Analysis of Elastic High-Speed Vehicles," *Journal of Guidance, Control, and Dynamic*, Vol. 20, No. 1, 1995, pp. 87-95.
- [5] Buschek, H., and Calise, A. J., "Uncertainty Modeling and Fixed-Order Controller Design for a Hypersonic Vehicle Model," *Journal of Guidance, Control, and Dynamic*, Vol. 20, No. 1, 1997, pp. 42-48.
- [6] Heeg, J., Gilbert, M. G., and Pototzky, A. S., "Active Control of Aerothermoelastic Effects for a Conceptual Hypersonic Aircraft," *Journal of Aircraft*, Vol. 30, No. 4, 1993, pp. 453-458.
- [7] R. Lind., "Linear Parameter-Varying Modeling and Control of Structural Dynamics With Aerothermoelastic Effects," *Journal of Guidance, Control, and Dynamic*, Vol. 25, No. 4, 2002, pp. 733-739.
- [8] An, H., Liu, J. X., and Wang, C. H., "Disturbance Observer-Based Antiwindup Control for Air-Breathing Hypersonic Vehicles," *IEEE Transactions on Industrial Electronics*, Vol. 63, No. 5, 2016, pp. 1-1.
- [9] Wu, G. H., and Meng, X. Y., "Nonlinear Disturbance Observer Based Robust Backstepping Control for a Flexible Air-Breathing Hypersonic Vehicle," *Aerospace Science and Technology*, Vol. 54, 2016, pp. 174-182.
- [10] Liu, Z., Tan, X., and Yuan, R., "Immersion and Invariance-Based Output Feedback Control of Air-Breathing Hypersonic Vehicles," *IEEE Transactions on Automation Science and Engineering*, Vol. 13, No. 1, 2016, pp. 394-402.
- [11] Karason, S.P., and Annaswamy, A. M., "Adaptive Control in the Presence of Input Constraints," *IEEE Transactions on Automatic Control*, Vol. 39, 1994, pp: 2325 - 2330.
- [12] Tao, G., and Kokotovic, P. V., "Adaptive Control of Systems with Actuator and Sensor Nonlinearities," *New York: Wiley*, 1996.
- [13] Xu, B., Guo, Y., Yuan, Y., and Fan, Y., "Fault-Tolerant Control Using Command-Filtered Adaptive Back-Stepping Technique: Application to Hypersonic Longitudinal Flight Dynamics," *International Journal of Adaptive Control and Signal Processing*, Vol. 30, No. 4, 2015, pp. 553-577.
- [14] Su, X., and Jia, Y., "Constrained Adaptive Tracking and Command Shaped Vibration Control of Flexible Hypersonic Vehicles," *IET Control Theory and Applications*, Vol. 9, No. 12, 2015, pp. 1857-1868.
- [15] Chen, M., Ge, S. S., and Ren, B. B., "Adaptive Tracking Control of Uncertain MIMO Nonlinear Systems With Input Constraints," *Automatica*, Vol. 47, No. 3, 2011, pp. 452-465.
- [16] Wang, F., Zou, Q., and Hua, C., "Disturbance Observer-Based Dynamic Surface Control Design for a Hypersonic Vehicle With Input Constraints and Uncertainty," *Proceedings of the Institution of Mechanical Engineers*, Vol. 230, No. 6, 2016, pp. 522-536.
- [17] Bu, X. W., Wu, X. Y., and Tian, M. Y., "High-Order Tracking Differentiator Based Adaptive Neural Control of a Flexible Air-Breathing Hypersonic Vehicle Subject to Actuators Constraints," *ISA Transactions*, Vol. 58, 2015, pp. 237-247.

- [18] Zhou, Q., Li, H. Y., Wang, L. J., and Lu, R. Q., "Prescribed Performance Observer-Based Adaptive Fuzzy Control for Nonstrict-Feedback Stochastic Nonlinear Systems," *IEEE Transactions on Systems, Man, and Cybernetics: Systems*, Vol. PP, No. 99, 2017, pp: 1-12.
- [19] Xu, B., "Robust Adaptive Neural Control of Flexible Hypersonic Flight Vehicle With Dead-Zone Input Nonlinearity," *Nonlinear Dynamics*, Vol. 80, No. 3, 2015, pp. 1509-1520.
- [20] Yang, Q., and Chen, M., "Adaptive Neural Prescribed Performance Tracking Control for Near Space Vehicles With Input Nonlinearity," *Neurocomputing*, Vol. 174, 2016, pp. 780-789.
- [21] Chen, M., Ge, S. S., and How, B. V. E., "Robust Adaptive Neural Network Control for a Class of Uncertain MIMO Nonlinear Systems With Input Nonlinearities," *IEEE Transactions on Neural Networks*, Vol. 21, No. 5, 2010, pp. 796-812.
- [22] Zhou, Q., Wang, L. J., Wu, C. W., et al. "Adaptive Fuzzy Tracking Control for a Class of Pure-Feedback Nonlinear Systems With Time-Varying Delay and Unknown Dead Zone," *Fuzzy Sets and Systems*, Vol: 329, 2016, pp: 36-60.
- [23] Hu, Q. L., Meng, Y., "Adaptive Backstepping Control for Air-breathing Hypersonic Vehicle With Actuator Dynamics," *Aerospace Science and Technology*, Vol. 67, 2017, pp. 412-421.
- [24] Li, Z., Zhou, W., and Liu, H., "Nonlinear Robust Control of Hypersonic Aircrafts With Interactions Between Flight Dynamics and Propulsion Systems," *ISA Transactions*, Vol. 64, 2016, pp. 1-11.
- [25] Fiorentini, L., Serrani, A., and Bolender, M. A., "Nonlinear Robust Adaptive Control of Flexible Air-Breathing Hypersonic Vehicles," *Journal of Guidance, Control, and Dynamic*, Vol. 32, No. 2, 2009, pp. 402-417.
- [26] Parker, J. T., Serrani, A., and Yurkovich, S., "Control-Oriented Modeling of an Air-Breathing Hypersonic Vehicle," *Journal of Guidance, Control, and Dynamic*, Vol. 30, No. 3, 2007, pp. 856-869.
- [27] Tong, S. C., Li, Y. M., Sui, S., "Adaptive Fuzzy Tracking Control Design for SISO Uncertain Nonstrict Feedback Nonlinear Systems," *IEEE Transactions on Fuzzy Systems*, Vol. 24, No. 6, 2016, pp: 1441 – 1454.
- [28] Wang, H. Q., Chen, B., and Lin, C., "Adaptive Neural Tracking Control for a Class of Stochastic Nonlinear Systems," *International Journal of Robust and Nonlinear Control*, Vol. 24, No. 7, 2014, pp. 1262–1280.
- [29] Zhou, J., Wen, C., and Zhang, Y., "Adaptive Output Control of Nonlinear Systems With Uncertain Dead-Zone Nonlinearity," *IEEE Transactions on Automatic Control*, Vol. 21, No. 3, 2006, pp. 504-511.
- [30] Wu, B., Cao, X., and Xing, L., "Robust Adaptive Control for Attitude Tracking of Spacecraft With Unknown Dead-Zone," *Aerospace Science and Technology*, Vol. 45, 2015, pp. 196-202.
- [31] Chen, W. H., and Guo, L., "Analysis of Disturbance Observer Based Control for Nonlinear Systems Under Disturbances With Bounded Variation," *Proceedings of International Conference on Control*, 2004, pp. 1-5.
- [32] Polycarpou, M., Farrell, J., and Sharma, M., "On-Line Approximation Control of Uncertain Nonlinear Systems: Issues With Control Input Saturation," *American Control Conference*, Vol.1, 2003, pp. 543-548.
- [33] Swaroop, D., Hedrick, J. K., Yip, P. P., and Gerdes, J. C., "Dynamic Surface Control for a Class of Nonlinear

Systems," *IEEE Transactions on Automatic Control*, Vol. 45, No. 10, 2000, pp. 1893-1899.

ACCEPTED MANUSCRIPT